

Automatic footprint detection approach for the calculation of arch index and plantar pressure in a flat rubber pad

Ke-Han Su¹ · Thossaporn Kaewwichit² ·
Chien-Hsun Tseng³ · Chong-Ching Chang²

Received: 14 January 2015 / Revised: 18 June 2015 / Accepted: 29 June 2015 /

Published online: 1 August 2015

© Springer Science+Business Media New York 2015

Abstract To obtain the Arch Index (AI) of footprint, the operation process through a Flat Rubber Pad (FRP) is manually time consuming to realize the necessary foot contact area. To deal with the problem, this paper developed an automatic footprint detection approach by employing the Otsu's thresholding method and the three components of HSV color space to segment the foot contact boundary in a footprint image. In addition, the ink density pattern of the FRP footprint image represents the pressure with a qualitative description of plantar pressure; the higher the ink density, the higher the pressure. Based on the principle, this paper examined the relationship between the intensity of the gray footprint image and body weight so as to quantify the magnitude of plantar pressures. Therefore, the depths of ink on the footprint image are used for plantar pressure calculation. The experiments verified that the proposed approach incorporated with the FRP can simultaneously obtain both the arch index and the plantar pressure with better accuracy when compared with other existing methods. The advantages of the developed approach with the FRP are that it can help reduce operating time and cost, and automatically obtain the foot contact area for further foot-related calculation without clinical expertise.

Keyword Flat rubber pad · Automatic footprint detection · Plantar pressure · Arch index

✉ Chong-Ching Chang
jeff0718@mail.nutn.edu.tw

¹ Department of Mechanical and Energy Engineering, National Chiayi University, Chiayi City, Taiwan 60004, Republic of China

² Graduate Institute of Mechatronic System Engineering, National University of Tainan, Tainan, Taiwan 70005, Republic of China

³ Department of Information Engineering, Kun Shan University, Tainan, Taiwan 71070, Republic of China

1 Introduction

The foot is the most important foundation for the human body to support, balance, and transmit the body's weight to the ground which allows locomotion. It absorbs the impact force during activity which would affect lower limbs such as the knees [12], pelvis [11], and even the spine [2]. In practice, foot posture and functions are considered to be an assessment of the structural characteristics of the foot. It is used to analyze the influence of lower limb, gait pattern, body balance and functional ability for lower limb treatment and injury prevention [23, 25] or for generating a proper-fitting foot orthotic [10]. To calculate the foot-function indexes such as Arch Index (AI) [4], Arch Angle [27], and Stahelis Arch Index [21] et al., the ink footprint method has been widely used in clinical and research settings. For instance, the Flat Rubber Pad (FRP) is impregnated with ink underlying the paper to acquire the necessary footprint, as illustrated in Fig. 1(a). To further calculate the foot-function indexes, the interested contact regions of foot are manually obtained by sketching along the footprint outline (as indicated in Fig. 1(b)), counting squares on a grid (as indicated in Fig. 1(c)), tracking the outline by planimeter [32] or using the graphics tablet [22]. However, these methods could be messy [33] and may not be suitable for routine operation due to human error and personal criteria. The manual process is also quite ineffective because the method of ink footprint acquisition is time-consuming and may require clinical expertise to assist measurement of foot functions, limiting its application in research and clinical settings.

As shown in Fig. 1, when standing, the whole body weight is supported by the feet. The footprint can be acquired through the FRP, where inks will be mostly placed at the location of higher pressure regions. The rubber pad is compressed by the applied load. The observable darker ink patterns represent the higher pressure regions. Different colors of ink intensities in the regions where the feet make ground contact are generated in accordance with variable values of contact pressures. The intensity of the ink pattern is proportional to the different amounts of loads from the body weight, yet this kind of footprint can indicate either high or low region pressure. The quantization value of pressures is not easy to be obtained.

To solve this constraint, a sensor-based measurement system, namely a Tactile system equipped with a fully conforming array pressure sensor, has been developed to provide and

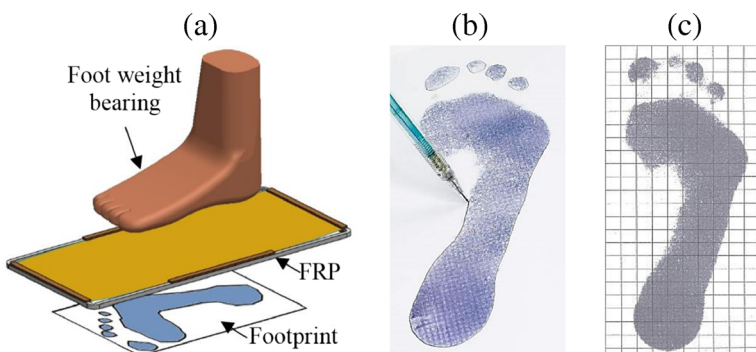


Fig. 1 Footprints obtained with the FRP: (a) the operation process of FRP; (b) manual outline tracing of footprint from FRP; (c) counting squares on a grid of footprint from FRP

analyze the quantitative data of plantar pressure for different foot-functions [8]. In the clinical setting, the Tactile system is widely used to quantify the high pressure areas in plantar pressure to further diagnose patients experiencing foot diseases and having lower extremity problems [3, 13]. Several researchers have assessed the efficiency of the sensor-based measurement system in terms of accuracy, repeatability and characteristics of measurement [9]. However, this system requires reliable software and user's technical skills, thus being highly costly. Moreover, it has been reported that the AI calculated from the sensor-based measurement cannot be used if the relative measurement error for isolated foot regions is not made [34].

The image-based plantar pressure measurement system equipped with a scanning machine (SM) has been designed to generate 2D images that schematically show details of the foot functions and evaluate the plantar pressure [15]. Drawn from the scanning technique, the plantar image can be acquired immediately. Like the sensor-based system, the SM system consists of complicated software. Expertise is then required, resulting in time-consuming evaluation of plantar pressure. In addition, the embedded scanners in the SM system always have low resolutions on the output image, which may affect the measurement accuracy. The plantar image from the SM system still needs manual contact area outlining. The automatic thresholding method in digital image processing has been widely used to detect the object's boundary. The concept of automatic thresholding is to separate the objects of interest from the background by automatically selecting an optimal threshold value based on the color/gray values in the image [26]. To our best knowledge, no automatic thresholding method that is applicable to all kinds of images has been discovered. Several image segmentation techniques have been proposed such as Otsu's thresholding method [26], image thresholding based on fuzzy set [19, 31] and color segmentation in several kinds of color space [7, 18]. Recently, the image segmentation technique has been widely used for medical or clinical research [5]. Yet, for foot function evaluation, image segmentation has rarely been applied for the detection of footprint contact area [24].

In this study, Otsu's thresholding method is used to automatically select the H, S, and V histograms threshold of the footprint image based on the HSV color space. After getting the binary images of the H, S, and V components, a combination of the above three binary images is developed for the automatic footprint detection system (AFDS). Subsequently, the segmentation image obtained from the combined binary image and the original image can be conducted to evaluate the magnitude of plantar pressure with its proportion to body weight. To evaluate accuracy of the segmentation technique, calculated AI and plantar pressure, the performance of image segmentation, AI and plantar pressure are compared with the traditional footprint method (i.e., outlined manually) and the commercial pressure measurement system (i.e., Tactile system). Experimental results verified that the developed automatic footprint detection approach indeed can exhibit better accuracy than the classical Otsu's thresholding method in gray image processing. Moreover, the proposed approach incorporated with the FRP can simultaneously obtain both arch index and plantar pressure with better accuracy when compared with other existing methods.

The rest of this paper is organized as follows: Section 2 consists of the AI calculation and plantar pressure measurement, which describes the basic principle of the AI calculation and the plantar pressure measurement. Section 3 describes the developed AFDS in this paper. The experimental setup and results are discussed in section 4. The final section is the conclusions of this paper.

2 The introduction of ai calculation and plantar pressure measurement

2.1 AI calculation

In 1987, Cavanagh and Rogers developed an arch index (AI) [4]. To calculate the AI, the original footprint image is shown in Fig. 2(a). The total contact area including the toes (TCA) is arranged into the foot axis (the line from 2nd toe to heel) as illustrated in Fig. 2(b). Then, the foot contact area excluding the toes (FCA) is then divided into three equal parts (as indicates in Fig. 2(c)). The AI is calculated by the ratio of mid-foot area to the area of FCA as follows;

$$AI = \frac{B}{(A + B + C)}. \quad (1)$$

The AI was categorized into three types as high arch ($AI \leq 0.21$), normal arch (AI between 0.21 and 0.26), and low arch ($AI \geq 0.26$). The index has since been developed with a simple method to provide reliable and useful data for further clinical diagnosis, as there is a high correlation to navicular height [22], and pressure of the mid-foot [16].

2.2 Plantar pressure measurement

The human foot supports the whole body weight over a few contact areas of the plantar surface. This produces pressure under the foot reacting to the ground, which is so-called “plantar pressure”, the pressure acting between beneath the bare foot and ground contact during daily activities. The plantar pressure is relative to the anatomical structure of the human body over the foot. It plays an important role for patients who suffer from foot disease, injury or other healthcare related issues. Its assessment provides an indication of

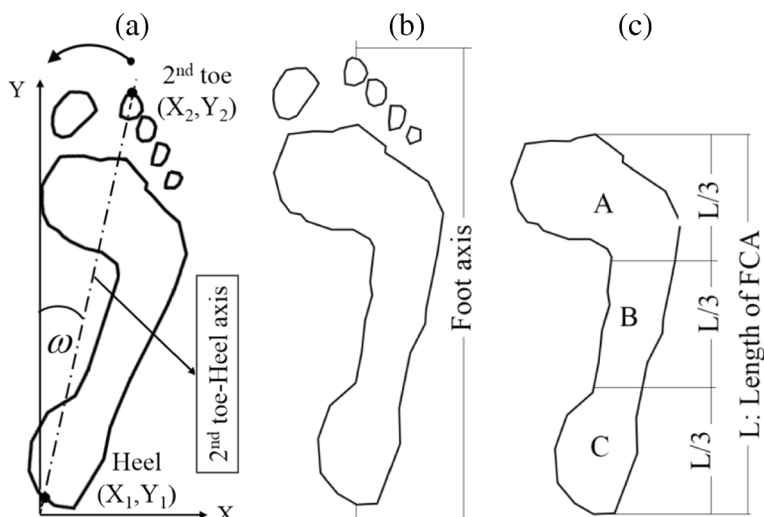


Fig. 2 Illustration of the rotation of footprint image from the 2nd toe-heel axis into X-Y coordinate: (a) original footprint image; (b) the total contact area including the toes (TCA) is arranged into the foot axis (the line from 2nd toe to heel); (c) The foot contact area excluding the toes (FCA) is then divided into three equal parts

the foot in gait and posture for diagnosing lower limbs. Several studies on plantar pressure measurement involve technology in sensor-based configuration [1] and image-based configuration [15]. Though the sensor-based measurement system (i.e., pressure platform system and in-shoe system) can provide more efficient, more flexible, and more mobile measurement techniques, it always requires reliable software, calibration, and maintenance. For lower cost devices, the image-based configuration has been developed for manufacturing customized insoles. The system provides the plantar image that transforms to plantar pressure by indicating the blood of the sole capillaries. However, such a kind of plantar pressure measurement mentioned above still requires complex devices and software, and clinical expertise.

3 Automatic footprint detection system

3.1 Image segmentation and color space selections

As is well known, no best image segmentation technique applicable to all images has been discovered. Therefore, several image segmentation techniques have been established [30]. Among various techniques, Otsu's method has received considerable attention. The method offers a better thresholding technique for general real world images with simplicity of implementation [29]. This technique is mostly performed in gray image, which is suitable for bimodal histograms and the calculations of the optimum threshold value that maximizes the between-class variances from the valley point of the histogram.

However, to apply Otsu's method on the footprint image with varying effect of applied pressure on the gray image (Fig. 3(a)), a common footprint with lower intensity on the mid-foot area is usually affected by lower pressure. The histogram of the image then contains the spreading valley area with unclear peaks of the histogram. To overcome this situation, the color image could provide the key information. Several color space systems such as RGB, HSV, and YCbCr color space systems, are available these days. The RGB color space is a common one, mostly used in hardware oriented applications by representing the primary colors of red (R), green (G), and blue (B). There are strong correlations surrounded by the R, G, and B components and the correlations fail to obtain satisfying effects. To reduce these correlations, various kinds of transforms have been proposed [20]. For the automatic color footprint detection system, all of the footprints are usually presented in a single color attribute, based on the purity of the color (varying of pressure). Therefore, this is closest to the HSV color system. In the HSV space, H refers to hue, S means saturation, and V refers to value. Let $i_{max} = \max(R, G, B)$, $i_{min} = \min(R, G, B)$ and $\delta = i_{max} - i_{min}$. The HSV color space is as follows [6]:

$$V = i_{max} \quad (2)$$

$$S = \begin{cases} 0, & \text{if } (i_{max} = 0) \\ \frac{\delta}{i_{max}}, & \text{otherwise,} \end{cases} \quad (3)$$

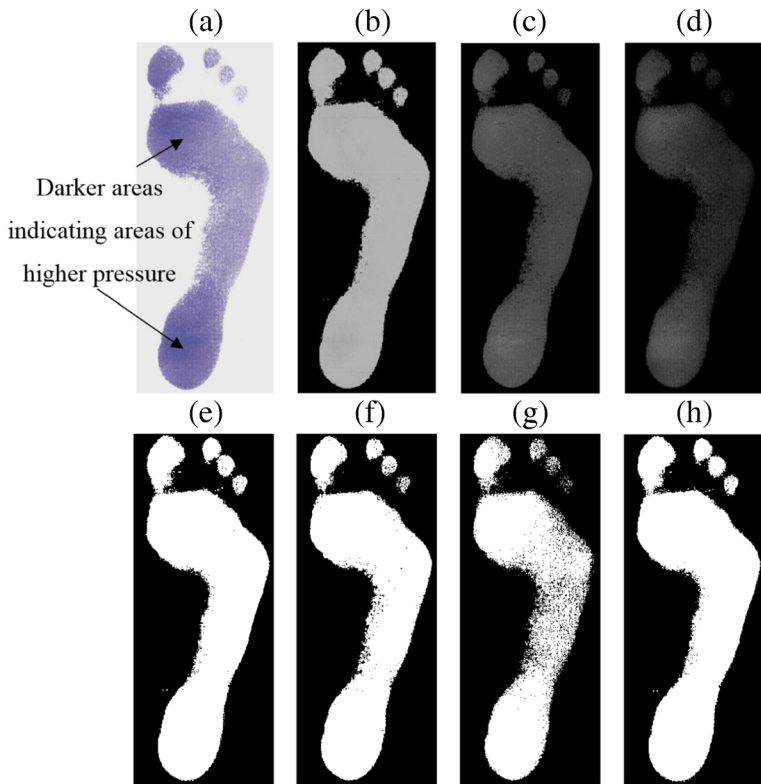


Fig. 3 The effect of high pressure areas on the footprint: (a) color image; (b) H component; (c) S component; (d) component; (e) the binary images of H component; (f) the binary images of S component; (g) the binary images of component; (h) the completed binary image

and

$$H = \begin{cases} \text{undefined}, & \text{if } S = 0 \\ \left(\frac{G-B}{\delta}\right) \times 60, & \text{if } (i_{max} = R) \\ \left(\frac{B-R}{\delta} + 2\right) \times 60, & \text{if } (i_{max} = G) \\ \left(\frac{R-G}{\delta} + 4\right) \times 60, & \text{if } (i_{max} = B) \end{cases} \quad (4)$$

Apparently, the value range of H, S, and V are $H \in [0, 360], S \in [0, 1]$, and $V \in [0, 1]$, respectively. The intensity of each component in H, S, and V is carried out. For the intensity of H, S, and V components, the H and S components represent the background on lower intensity value (nearly black color) and the object in higher intensity, while the V component represents background on the higher intensity value (nearly white color) and the object in lower intensity value. Thus, in order to indicate the intensity of images in the same system, the V component reverses (complements) the intensity value as follows:

$$V' = (1-V). \quad (5)$$

To segment the footprint image, the intensity images of the three components (see Figs. 3(b)—2(d)) are segmented by using Otsu's method for binary images (see Figs. 3(e)—2(g)). Therefore, the three binary images of H,S, and V' are in combination (see Fig. 3(h)) by using the union of the three components (σ) as follows:

$$\sigma = H \cup S \cup V' \quad (6)$$

3.2 Mathematical model of plantar pressure distribution

The principles of the plantar measurement system in the study of Chang et al. (2003, 2007) and Huang et al. (2011) were adopted for this study [15]. Changes in the blood flow through the capillaries of the sole represent the plantar pressure. The whiter the color is, the higher the pressure is. However, the plantar pressure distribution of the FRP could be indicated by the effect of high and low pressure areas on the footprint. The presence of varying pressure can be apparent through intensity patterns observable within the print. In this case, darker areas indicate areas of higher pressure (Fig. 3(a)). When the feet are placed on a platform's surface with the body physically supported, the level of the ink color in the gray image system on the print is directly proportional to the amount of the load built up on the sole. Involving the digital imaging system, the gray value G_k of the interested k -th region can be determined by the input image as:

$$G_k = \sum_{i=1}^m \sum_{j=1}^n (255 - g_{i,j}) \quad (7)$$

where $G_k, k \in [1, N]$ is the k -th region of the plantar surface A_k . The $g_{i,j}$ denote the gray level value of the pixel at any spatial coordinates $i \in [1, m], j \in [1, n]$ in the k -th region, and 255 is maximum gray level in the gray image system. Consequently, the sum of gray value G in all k -th regions can be calculated as:

$$G = \sum_{k=1}^N G_k \quad (8)$$

In this case, the total body weight W can be distributed to k -th region as:

$$W = \sum_{k=1}^N W_k \quad (9)$$

Therefore, we assume that the ratio of body weight is proportional with the ratio of gray value in k -th region as follows:

$$\frac{W_k}{W} \propto \frac{G_k}{G}, \quad (10)$$

Thus, the distribute load in k -th region W_k can be found from the relationship of gray value and the total body weight in the following equation as:

$$W_k = f \frac{G_k}{G} W, \quad (11)$$

where f , namely the adjustment factor is denoted as an adjustable factor based on conditions such as the general health and overall physical activity of the subject, as well as relative measurement error. The adjustment factor f is assumed to predict further conditions. For example, body weight during locomotion can be approximated to be three to six times that of normal conditions [14], whereas the pressure of one foot landing on the heel region could be one and half times that of one foot standing [17]. However, this study did not take such an adjustment into account. For this particular paper, which studied automatic detection for the AI and plantar pressure calculation, the adjustment factor is set to 1.

Hence, the pressure P_k at the k -th region of the plantar surface A_k can be equated by the forces presented by distributed body weight W_k across A_k , and it may be characterized by four components: W , G_k , G , and A_k as:

$$P_k \equiv \frac{W_k}{A_k} = f \frac{G_k}{A_k G} W \quad (12)$$

Having the image of the sole transformed to the gray binary code, the local plantar pressure P_k can then be calculated in an effective and efficient manner by adopting Eq. (12).

3.3 Automatic footprint detection system (AFDS)

The AFDS was established to achieve the contact areas where the system can automatically calculate the AI and the plantar pressure. A process flow of the AFDS is illustrated in Fig. 4, which describes tasks of processing as follows:

- (I) Using a color footprint image as an input image.
- (II) Obtaining the contact areas by the image segmentation technique mentioned above.
- (III) Rotating the raw footprint image to the 2nd toe-heel axis as depicted in Fig. 2(b) for AI and plantar pressure calculation. The rotation angle (ω) can be found as follows:

$$\omega = \tan^{-1} \frac{X_2 - X_1}{Y_2 - Y_1}. \quad (13)$$

- (IV) Providing the contact area of the sole of the foot, the plantar image shown in Fig. 2(b) is divided into 4 main regions: heel, mid-foot, metatarsal, and toe according to the calculation of the Cavanagh's AI. These areas can physically support most of the body weight and are constantly adjusted by the body's balance.
- (V) Having the full body weight obtained.
- (VI) Obtaining the calibration factor, however, the A_k is still in image coordinates. To convert the A_k to actual scale, it can be converted by the calibration factor φ with the known actual scale as following:

$$\varphi = \frac{l_a}{l_p}, \quad (14)$$

where l_a is the actual length of known actual scale and l_p is the length of pixel.

- (VII) The sole image is converted into 8-bit gray scale for calculating the plantar pressure which can be immediately measured by adopting Eq. (12).

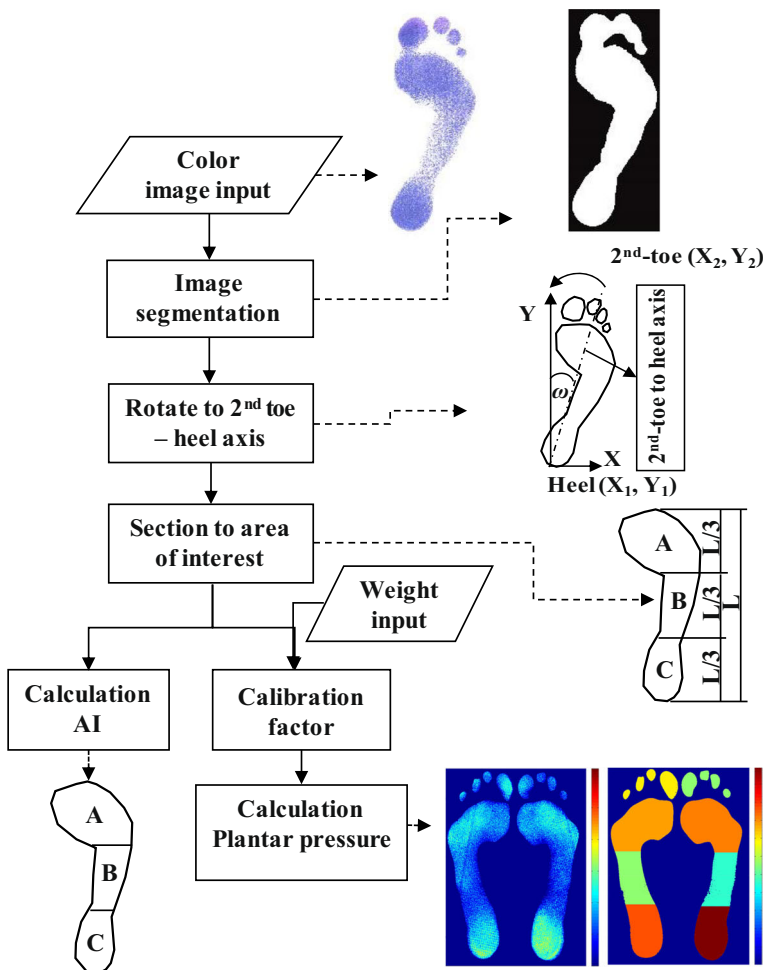


Fig. 4 The process flow of the AFDS

4 Experimental setup and results

This section describes the experimental setup and results of the performance of the image segmentation, AI calculation, and plantar pressure distribution. To calculate the plantar information, Urry and Wearing first exploited the FRP system for footprint acquisition in 2001 [32]. In this paper, the FRP system shown in Fig. 5(a) was used as an experimental platform to evaluate the performance of the proposed approach. In the experimental FRP system, the size of the inside rubber pad is 355 mm x 165 mm with a 1.5 mm thickness. Figure 5 shows the process of FRP operation. Before using the FRP, the rubber pad was prepared by spreading ink on the pad surface (as indicated in Fig. 5(a)). Firstly, the tested subject stands firmly in front of the platform in preparing for measurement of the footprint and then places the right foot on the ground supporter (as shown in Fig. 5(b)). Next, the left foot is put lightly on the pad, then the subject stands firmly on the platform, while looking straight ahead at eye-level above a specific point to obtain the left footprint (as shown in Fig. 5(c)). After that, the left foot is removed to the ground (as indicated in

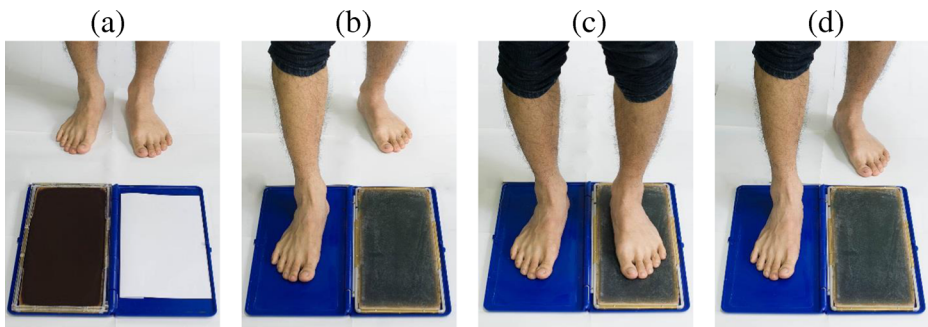


Fig. 5 Process of FRP operation for obtaining footprint (for the case of left footprint)

Fig. 5(d) and the right foot taken back. Similarly, the same procedure can be used for obtaining the right footprint. If during acquiring the footprint, the subject noticeably swayed excessively or the ink on the print was smeared, then the footprint was discarded. In addition, five footprints were repeated on each foot for each subject. Three similar pressure patterns were selected and used to calculate the mean pressure. In the experiments, the tested subjects were 20 healthy males with an average of 24.9 years old, 68.9 kg, and 163.8 cm. Without loss of generality, the test subjects were selected based on having not experienced a lower-limb injury.

4.1 Performance of image segmentation

In the experiments, 120 footprints obtained from 20 tested subjects were used as the test samples. The contact areas of each footprint were determined using five different boundary search methods. They were: (1) the traditional footprint method (TFM, as the gold standard reference method), (2) a manual user's decision method with the scale 0.5 cm/point ($M_{0.5}$), (3) a manual user's decision method with the scale 1 cm/point (M_1), (4) Otsu's thresholding method, and (5) the proposed method (HSV_Otsu), respectively. The TFM method was used to outline the foot boundary by pencil and then a PC scanner was used to scan the footprint paper into a JPEG format file (as indicated in Fig. 6(a)). In the JPEG format, by using Adobe Photoshop CS5 software (Adobe Systems Incorporated, USA), the foot boundary can be traced using Lasso Tool. The white color and black color then plainly represent the inner outline and outer outline of the contact area, respectively. After that, the white color area was exploited to calculate the contact area as a reference area (as shown in Fig. 6(b)).

In addition, the specific manual user's decision method was constructed for two scales $M_{0.5}$ (as shown in Fig. 6(c)) and M_1 (as shown in Fig. 6(d)) by using the MATLAB 2012a (Math Works, USA) image processing toolbox. In this paper, the manual method with two scales $M_{0.5}$ and M_1 was used to simulate a user's decision in different point resolutions. Moreover, before exploiting the aforementioned methods, all footprints were arranged with a foot axis (i.e., an axis from 2nd toe to heel, as indicated in Fig. 2(b)) and divided into six areas: toes, forefoot (A), mid-foot (B), heel (C), FCA, (as indicates in Fig. 2(c)), and TCA (as indicates in Fig. 2(b)).

Furthermore, to evaluate the performance of segmentation images, a misclassification error with parameter η [30] is used. That is,

$$\eta(\%) = 100 \times \frac{|B_o \cap B_T| + |F_o \cap F_T|}{|B_o| + |F_o|}, \quad (15)$$

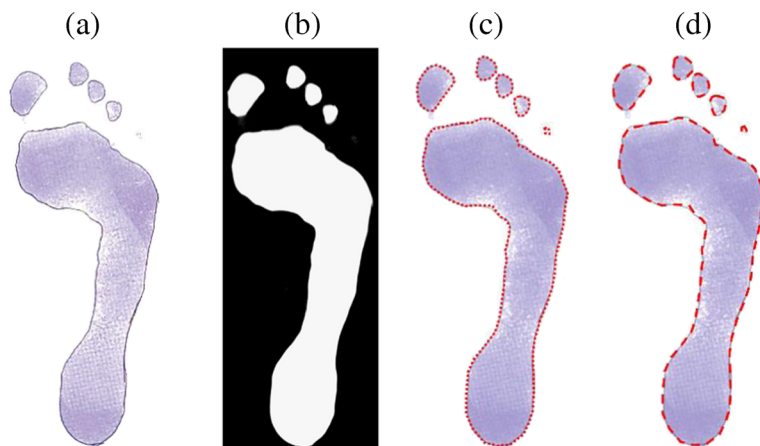


Fig. 6 The different FRP footprints: (a) original image obtained by TFM; (b) the white color contact area (as the gold standard); (c) manual method with scale $M_{0.5}$; (d) manual method with scale M_1

where B_o and F_o are background and foreground of original (ground-truth) image, B_T and F_T are background and foreground area pixels in the resulting image, and $|.|$ is the set cardinality.

Figure 7 shows the different segmentation images of footprints obtained through different methods. Table 1 shows the comparisons of performance index $\eta(\%)$ of segmentation image on different areas with different methods. Note that in Table 1, the gold standard image is used as the reference as indicated in Fig. 6(b). As shown in Table 1, boundary search methods also can be categorized into two groups, the manual method ($M_{0.5}$ and M_1) and the automatic thresholding method (Otsu and HSV_Otsu). According to the Table 1, the manual method shows better performance on the experiment results for different areas of the footprint. This, however, involves drawbacks such as user error or criteria, and operation time (the result of the mean computational time for different methods is shown in Table 2). To overcome the above problems, it is necessary to use the automatic thresholding method. In the lower part of

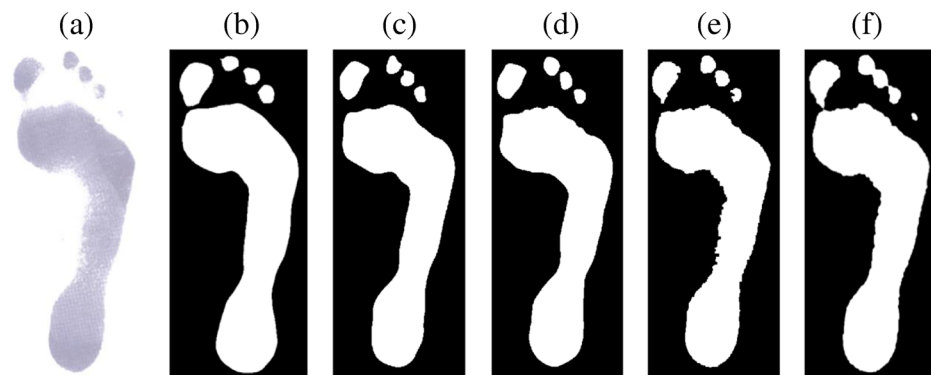


Fig. 7 Examples of segmentation images: (a) original image; (b) gold standard; (c) $M_{0.5}$; (d) M_1 ; (e) Otsu method; (f) with the HSV_Otsu method

Table 1 Performance comparisons for different methods with the gold standard image

Technique groups	Methods	TCA (%)	FCA (%)	A (%)	B (%)	C (%)	Toes (%)	Mean (%)
Manual methods	M _{0.5}	97.52	98.17	98.73	96.41	97.64	97.30	97.62
	M ₁	98.30	98.50	98.58	96.94	98.22	97.10	97.94
Automatic thresholding methods	Otsu	96.38	97.14	95.71	94.2	97.83	96.15	96.23
	HSV_Otsu (proposed)	97.90	98.67	97.56	98.23	98.73	99.23	98.38

Table 1, it can be found that the HSV_Otsu method showed higher average performance on all areas of the footprint than the one using Otsu.

4.2 Performance of AI calculation

In this subsection, the performance of AI calculation was evaluated for different methods, and compared to the gold standard method TFM. To evaluate the performance of AI, the performance index mean standard error (MSE) [28] was used in this paper. The MSE was defined as follows:

$$\text{MSE} = \frac{1}{n} \sum_{i=1}^n (f_i - y_i)^2, \quad (16)$$

where f_i is the prediction, and y_i is the true value (or the reference value).

For the AI calculation, area B was the key point to be considered. In most cases, this area was affected by the lower pressure from the body weight, resulting in lower color intensity over this area. In this situation, the histogram on the gray image would reveal another peak of gray intensity. As shown in Table 1, it can be found that the HSV_Otsu method had better ability on segmentation at mid-foot area B due to using additional components H and S. Therefore, it is believed that using the HSV_Otsu method can provide better estimation performance on AI calculation than other methods. The comparisons of calculation performance are shown and listed in Fig. 7 and Table 3, respectively. According to the experimental results shown in Table 3 and Fig. 8, it can be found that the proposed approach indeed had better performance ability on AI calculation than others, either on the performance index mean \pm SD deviation or MSE.

In Table 1, it was shown that the performance on HSV_Otsu method was better than Otsu's method at mid-foot area B. This is because the H and S components in HSV space can be used to detect the object by detecting the colors when these color intensities have narrow ranges laying on the histograms. Therefore, the H and S components can provide suitable bimodal histograms effectively by using Otsu's method to select the thresholding value. Thus, the HSV_Otsu method can provide better performance on the mid-foot region of automatic

Table 2 Comparison of the mean computational time for different methods

	M _{0.5}	M ₁	Otsu	HSV_Otsu
Operation time (sec.)	51.94	40.03	0.18	0.67

Table 3 AI results on Mean \pm SD and MSE performance for different methods with the TFM as ground-truth images

		Left foot	Right foot
TFM (Reference)	Mean \pm SD	0.240 ± 0.031	0.237 ± 0.027
M _{0.5}	Mean \pm SD	0.234 ± 0.028	0.236 ± 0.028
	MSE	0.417×10^{-4}	0.411×10^{-4}
M ₁	Mean \pm SD	0.234 ± 0.028	0.236 ± 0.028
	MSE	0.417×10^{-4}	0.428×10^{-4}
Otsu	Mean \pm SD	0.207 ± 0.048	0.224 ± 0.044
	MSE	9.500×10^{-4}	10.487×10^{-4}
HSV_otsu (proposed)	Mean \pm SD	0.234 ± 0.030	0.239 ± 0.032
	MSE	0.108×10^{-4}	0.093×10^{-4}

thresholding method and showed better performance index MSE on the AI (as indicates re AI result in Table 3 and it is illustrated corresponding to Fig. 8).

4.3 Performance of plantar pressure distribution

To evaluate the performance of the calculated plantar pressure distribution from the proposed HSV_Otsu method with the FRP, the tactile pressure platform (TP) (Tactilus, Pressure Mapping System, Madison, USA) was used as the standard reference system in this paper. The size of sensor point and number of the grid is 40.894 cm x 40.894 cm, 1.278 cm x 1.278 cm, and 32×32 units, respectively. In addition, the SM system was also conducted to calculate the plantar pressure distribution for the purpose of comparison. In the experiments, to calculate the plantar pressure distribution, the regions of the footprint are also divided into five areas in advance. However, on plantar pressure calculation, only three main contact areas need to be considered: forefoot, mid-foot, and heel. Figure 9 shows the evaluation of the plantar pressure obtained from the proposed approach and TP system, respectively. Table 4 lists the mean \pm SD of mean plantar pressure for different measurement systems on different regions. Figure 10 shows the comparisons of the performance index MSE for different measurement systems with the standard reference system TP on both feet. According to Table 4 and Fig. 10, it can be found that in the forefoot area, the measurement difference between the SM system and the proposed system was small (less than 0.010 of the MSE value). However, the

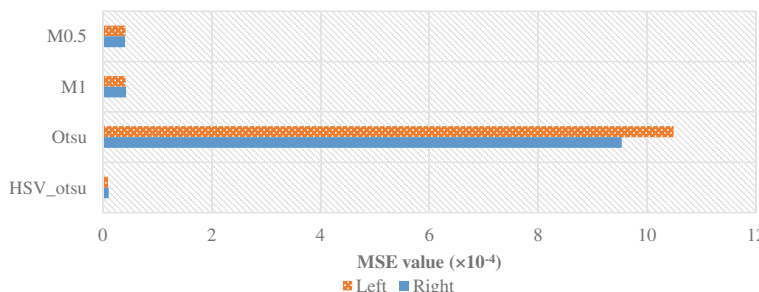


Fig. 8 The performance index MSE on AI calculation for different methods compared with the standard reference (on Left Foot and Right Foot)

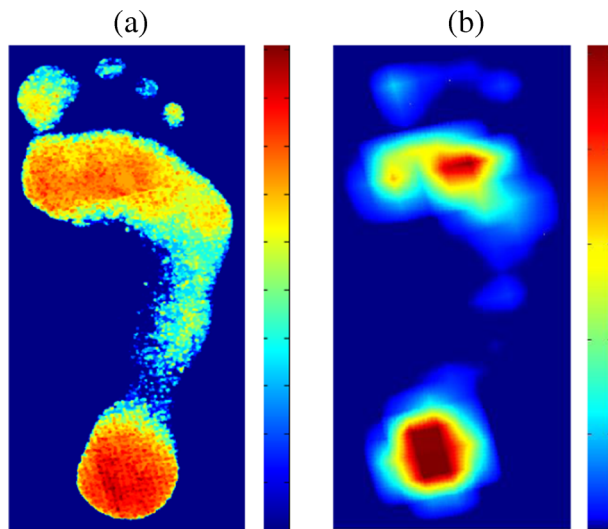


Fig. 9 The Plantar pressure evaluation obtained from: (a) the proposed approach (HSV_Otsu with FRP); (b) TP system

measurement differences between the SM system and the proposed system were large in the mid-foot and heel areas. For instance, in the mid-foot area, the proposed approach performs in good agreement with the reference TP (0.009 MSE value at most), while the SM system performs at a higher MSE value (0.048 at most). Similarly, the data obtained in the heel area also indicated that the proposed approach also exhibits better ability on plantar pressure calculation. This was because the proposed approach (within FRP) can directly transfer the load through the rubber pad. Therefore, it can provide better results in all regions than SM system which indicated the plantar pressure by the intensity level of the blood capillaries of the sole.

In short, the FRP system combined with the proposed Otsu_HSV method can provide better performance in the automatic detection of the foot contact area when compared with the traditional manual tracing outline, $M_{0.5}$, M_1 techniques, and the classical Otsu's thresholding method. In addition, the results demonstrated that it also can provide superior ability on AI calculation and plantar pressure evaluation simultaneously.

Table 4 The comparisons of mean plantar pressure on different areas with different measurement systems (unit : N/cm²)

Systems	Left foot			Right foot		
	Forefoot	Mid-foot	Heel	Forefoot	Mid-foot	Heel
TP (Reference)	Mean ± SD	0.43 ± 0.06	0.25 ± 0.13	0.65 ± 0.13	0.46 ± 0.06	0.26 ± 0.14
SM	Mean ± SD	0.36 ± 0.04	0.41 ± 0.05	0.39 ± 0.04	0.39 ± 0.04	0.42 ± 0.05
	MSE	0.009	0.042	0.082	0.01	0.048
Proposed	Mean ± SD	0.38 ± 0.08	0.32 ± 0.11	0.52 ± 0.09	0.41 ± 0.09	0.29 ± .10
	MSE	0.009	0.009	0.036	0.009	0.005

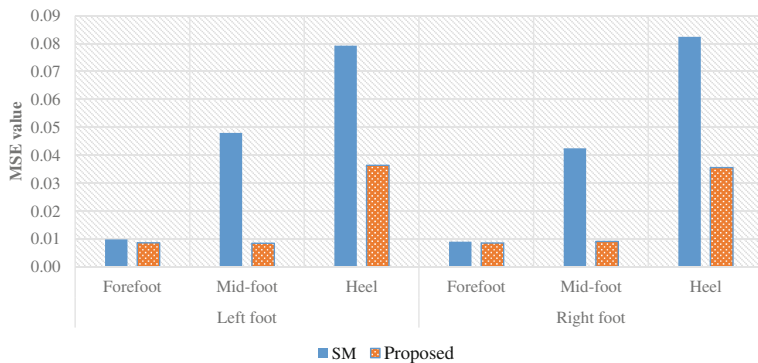


Fig. 10 The MSE corresponding graphical of MSE performance based on comparison of their plantar pressure results with the reference TP

5 Conclusion

In this paper, an automatic footprint detection approach is presented based on Otsu's thresholding method with HSV color space which is applied for a footprint through Flat Rubber Pad (FRP). This approach is used in segmentation of the footprint image for the necessary foot contact area to calculate the AI. In addition, the segmented image was used to evaluate the plantar pressure via the effect of varying ink density and the high pressure areas on the FRP footprint from the qualitative description so as to quantify plantar pressures magnitude. The experimental results showed better performance on automatic footprint detection and AI calculation compared with other existing methods. The evaluated plantar pressure magnitude performance closely agreed with the commercial pressure platform system, but outperformed the previous scanning machine system. Therefore, the proposed approach provides an option to overcome the drawbacks of a time-consuming and manual operation that involves human error, which can be operated without clinical expertise in order to obtain the necessary foot contact area on the ink footprint method through the FRP when compared with the traditional manually outline. Most importantly, the advantages of the proposed Automatic Footprint Detection System (AFDS) are being economical with less operation time, plus the ability to provide accurate contact area, AI and quantify plantar pressure magnitude when compared with commercial systems.

Acknowledgments The authors would like to thank the Ministry of Science and Technology of the Republic of China, Taiwan, for support of this research under Grant Nos. NSC101-2221-E-024-002 and MOST 103-2221-E-415 -031. In particular, the authors would like to thank Dr. Prapai Jantrasakul for her assistance in English writing.

References

1. Abdul Razak AH, Zayegh A, Begg RK, Wahab Y (2012) Foot plantar pressure measurement system: A review. Sensors 12(7):9884–9912
2. Bird AR, Payne CB (1999) Foot function and low back pain. Foot 9(4):175–180
3. Bus SA, Ulbrecht JS, Cavanagh PR (2004) Pressure relief and load redistribution by custom-made insoles in diabetic patients with neuropathy and foot deformity. Clin Biomech 19(6):629–638

4. Cavanagh PR, Rodgers MM (1987) The arch index: a useful measure from footprints. *J Biomech* 20:547–551
5. Chae SH, Moon HM, Chung Y, Shin J, Pan SB (2014) Automatic lung segmentation for large-scale medical image management. *Multimedia Tools Appl.* doi:[10.1007/s11042-014-2201-1](https://doi.org/10.1007/s11042-014-2201-1)
6. Chen W, Shi YQ, Xuan G (2007) Identifying computer graphics using HSV color model and statistical moments of characteristic functions. In: Proceedings of IEEE International Conference on Multimedia and Expo. 1123–1126
7. Cheng HD, Jiang XH, Sun Y, Wang J (2001) Color image segmentation: advances and prospects. *Pattern recognition. Pattern Recogn* 34(12):2259–2281
8. Chevalier TL H, Hodgins H, Chockalingam N (2010) Plantar pressure measurements using an in-shoe system and a pressure platform: A comparison. *Gait Posture* 31(3):397–399
9. Chevalier TL, Hodgins H, Chockalingam N (2010) Plantar pressure measurements using an in-shoe system and a pressure platform: A comparison. *Gait Posture* 31(3):397–399
10. Chuckpaiwong B, Nunley JA, Mall NA, Queen RM (2008) The effect of foot type on in-shoe plantar pressure during walking and running. *Gait Posture* 28(3):405–411
11. Franco AH (1987) Pes cavus and pes planus analyses and treatment. *Phys Ther* 67(5):688–694
12. Gross KD, Felson DT, Niu J, Hunter DJ, Guermazi A, Roemer FW, Dufour AB, Gensure RH, Hannan MT (2011) Association of flat feet with knee pain and cartilage damage in older adults. *Arthritis Care Res* 63(7):937–944
13. Hessert MJ, Vyas M, Leach J, Hu K, Lipsitz LA, Novak V (2005) Foot pressure distribution during walking in young and old adults. *BMC Geriatr* 5(1):8
14. Hills AP, Hennig EM, McDonald M, Bar-Or O (2001) Plantar pressure differences between obese and non-obese adults: a biomechanical analysis. *J Int Assoc Study Obes* 25(11):1674–1679
15. Huang CN, Lee MY, Chang CC (2011) Computer-aided design and manufacturing of customized insoles. *Comput Graph Appl IEEE* 31:74–79
16. Jonely H, Brismée JM, Sizer PS Jr, James CR (2011) Relationships between clinical measures of static foot posture and plantar pressure during static standing and walking. *Clin Biomech* 26(8):873–879
17. Kellis E (2001) Plantar pressure distribution during barefoot standing, walking and landing in preschool boys. *Gait Posture* 14(2):92–97
18. Lin XL, Zhong W, Zhong WX (2009) Research of double-threshold segmentation of brazing-area defect of saw based on Otsu and HSV color space. In: International Congress on Image and Signal Processing, CISIP'09. 2nd, IEEE 1–4
19. Lopes NV, Couto PA M d, Bustince H, Melo-Pinto P (2010) Automatic histogram threshold using fuzzy measures. *Image Process IEEE Trans* 19(1):199–204
20. Luccheseyz L, Mitray SK (2001) Color image segmentation: A state-of-the-art survey. *Proc Indian Natl Sci Acad (INSA-A)* 67(2):207–221
21. Mathieson I, Upton D, Birchenough A (1999) Comparison of footprint parameters calculated from static and dynamic footprints. *Foot* 9(3):145–149
22. McCrory JL, Young MJ, Boulton AJM, Cavanagh PR (1997) Arch index as a predictor of arch height. *Foot* 7(2):79–81
23. Menz HB, Fotoohabadi MR, Wee E, Spink MJ (2012) Visual categorisation of the arch index: a simplified measure of foot posture in older people. *J Foot Ankle Res* 5(1):1–7
24. Mora M, Sbarbaro D (2005) A robust footprint detection using color images and neural networks. In: Progress in Pattern Recognition, Image Analysis and Applications 311–318
25. Nigg BM, Cole GK, Nachbauer W (1993) Effects of arch height of the foot on angular motion of the lower extremities in running. *J Biomech* 26:909–916
26. Otsu N (1975) A threshold selection method from gray-level histograms. *Automatica*, 23–27
27. Razeghi M, Batt ME (2002) Foot type classification: a critical review of current methods. *Gait Posture* 15(3):282–291
28. Riaz S, Lee SW (2013) A robust multimedia authentication and restoration scheme in digital photography. *Multimedia Tools Appl* 73(4):1–31
29. Sahoo PK, Soltani SAKC, Wong AK (1988) A survey of thresholding techniques. *Comp Vision Graph Image Process* 41(2):233–260
30. Sezgin M (2004) Survey over image thresholding techniques and quantitative performance evaluation. *J Electron imaging* 13(1):146–168
31. Tizhoosh HR (2005) Image thresholding using type II fuzzy sets. *Pattern Recogn* 31(12):2363–2372

32. Urry SR, Wearing SC (2001) The accuracy of footprint contact area measurements: relevance to the design and performance of pressure platforms. *Foot* 11(3):151–157
33. Urry SR, Wearing SC (2001) A comparison of footprint indexes calculated from ink and electronic footprints. *J Am Podiatr Med Assoc* 91(4):203–209
34. Urry SR, Wearing SC (2005) Arch indexes from ink footprints and pressure platforms are different. *J Biomech* 15:68–73



Ke-Han Su received the Ph.D. degree in electrical engineering from National Cheng Kung University (NCKU), Tainan, Taiwan in 2008. From November 2009 to July 2012, he held a postdoctoral research position at the Department of electrical engineering of NCKU. From August 2012 to January 2014, he was an assistant researcher in the Electric Motor Technology Research Center at NCKU. Since February 2015, he joined the Department of Mechanical and Energy Engineering, National Chiayi University, Chiayi City, Taiwan, where he is currently an assistant professor. His research interests include CNC motion control, intelligent control systems, and mechatronics. He is also a member of the IEEE Industrial Electronics Society.



Thossaporn Kaewwachit received the B.Eng. and M.Eng degree in production engineering from the King Mongkut's University of Technology North Bangkok, Bangkok, Thailand, in 2008 and 2010, respectively. He received the Ph.D. degree in electrical engineering from National University of Tainan, Tainan, Taiwan in 2015.



Chien-Hsun Tseng received the B.Sc. degree in applied mathematics from the National Cheng Kung University, Taiwan, the M.Math. degree from the University of New South Wales, Sydney, Australia, and the Ph.D. degree in electrical engineering from Curtin University of Technology, Perth, Australia, in 1995, 1997, and 2000, respectively. From 2000 to 2001, he was a Research Scientist at Weierstrass Institute for Applied Analysis and Stochastics (WIAS), Berlin, Germany. He joined the University of Warwick at Coventry, U.K., as a Research Fellow and then Senior Research Fellow from 2001 to 2004 and 2006 to 2008, respectively. From 2004 to 2006, he taught and researched as an Assistant Professor at Southern Taiwan University of Technology. He has been at the Kun Shan University, Taiwan since August 2008 where he is an Associate Professor in the Department of Information Engineering. His current research interests include: optimal digital and statistical filters design through optimization techniques, modeling of physical systems using digital signal processing techniques, digital image processing, VLSI, and sonar signal processing.



Chong-Ching Chang received his Ph.D. degree in mechanical engineering from the University of Pittsburgh, PA, U.S.A. He is currently a professor of the Graduate Institute of Mechatronic System Engineering National University of Tainan, Tainan, Taiwan.